Diamagnetic domains in beryllium observed by muon-spin-rotation spectroscopy

G. Solt and C. Baines
Paul Scherrer Institut, CH-5232 Villigen PSI, Switzerland

V. S. Egorov
Russian Research Center ''Kurchatov Institute,'' Moscow 123182, Russia

D. Herlach and U. Zimmermann
Paul Scherrer Institut, CH-5232 Villigen PSI, Switzerland

(Received 17 July 1998; revised manuscript received 29 October 1998)

Dia- and paramagnetic (Condon) domains were observed in single crystal beryllium for applied fields $\boldsymbol{H}\|[0001]$ of 1–3 T, at temperatures $T=0.1$–3 K, by muon-spin-rotation (μSR) spectroscopy at PSI. On varying H, the domains with magnetization parallel and opposite to $\boldsymbol{H}$ reappear in each de Haas–van Alphen period ΔH, detected by the doublet splitting in the precession frequency spectrum. As H varies within the ''domain section'' δH of a dHvA cycle, the domain inductions B_1, B_2 stay constant, while the volume fractions of the para- and diamagnetic regions vary linearly. The beat in the susceptibility amplitude $a(B)=4\pi(dM/dB)_{\max}$, with a period of $\approx 33\cdot\Delta H$, allowed us to determine B_i and δH for different regimes. As a increases by a factor of ≈ 3, the sections δH grow, $|B_2-B_1|\rightarrow\Delta H$, and the uniform state between two domain sections shows an increasingly strong diamagnetism, $-4\pi\chi\gg 1$. The domains persist up to $T\approx 3$ K and at fields down to $H\approx 1$ T. On varying H, a slight ''field overheating'' was observed. The domain area in the phase diagram is much larger than expected, while other predictions of the theory proved to be qualitatively correct. [S0163-1829(99)03509-2]

I. INTRODUCTION

The periodic formation of dia- and paramagnetic domains in nonmagnetic metals at low temperatures is a macroscopic manifestation of the interaction between electrons in quantized cyclotron orbitals, predicted by Condon.[1,2] The underlying physical background for Condon domains is the same as for the ''normal'' de Haas–van Alphen (dHvA) oscillations, the periodically emerging electronic Landau levels from below the Fermi surface, as the quantizing magnetic field $\boldsymbol{B}$ varies. For domain formation, in addition, the magnetic *interaction*[2] of electrons is essential: the field generated by an occupied Landau orbital is part of the quantizing field itself via $\boldsymbol{B}=\boldsymbol{H}+4\pi\boldsymbol{M}(\boldsymbol{B})$. Whether this self-consistency implies only a slight modification of the wave form of the oscillating magnetization or results in discontinuities, depends on the amplitude χ_a of the differential susceptibility $\chi=\partial M/\partial B$. (Here and in the following, M and B are the vector components along $\boldsymbol{H}$.) Besides crystal perfection and temperature, χ_a is determined by properties of the Fermi surface and the orientation and strength of $\boldsymbol{B}$. From the condition of thermodynamical stability

$$\partial H/\partial B=1-4\pi\chi>0 \tag{1}$$

it follows that sufficiently sharp dHvA oscillations having, for a field range, an amplitude

$$\chi_a(B,T)=(\partial M/\partial B)_{\max}>1/4\pi \tag{2}$$

will contain *thermodynamically unstable* sections within each dHvA cycle. Formally, the situation on the (H,B) plane corresponds to the (p,v) diagram of a real gas: at a given H *two* stable values B_1, B_2 exist, analogous to the specific volumes v_l, v_g in the liquid and the gas. Without external restriction on $\boldsymbol{B}$ (for a long cylinder oriented along $\boldsymbol{H}$), at a given $H=H_c$ the induction will vary discontinuously, jumping between $B_1\leftrightarrow B_2$ of equal free energies, leaping over a ''forbidden interval'' $\Delta B=B_2-B_1$ (like boiling at the equilibrium vapor pressure p_0). For a thin plate oriented *normal* to $\boldsymbol{H}$ (demagnetizing coefficient $n\approx 1$), the situation is different: the conservation of magnetic flux for a uniform sample would require $B=H$, even though for $B_1<H<B_2$ this implies an unstable value of B. What really happens[1] is that the uniform state breaks up and oppositely magnetized domains with induction B_1 and B_2, of a volume average $\overline{B}=H$, arise (''evaporation'' at a given total volume, $\overline{B}$ corresponding to the mean specific volume $\overline{v}$). This state with dia- and paramagnetic (or Condon) domains is analogous to the intermediate state of type 1 superconductors, the conflict between the quantum structure of the energy spectrum and the conservation of magnetic flux is in both cases ''solved'' by domain formation.

Since χ_a varies slowly with B, Eq. (2) holds normally over a field range with hundreds of dHvA cycles, each containing a section δH where domains coexist. The nature of the related recurrent phase transitions has attracted considerable theoretical interest.[3–8]

Until recently the only direct, spectroscopic evidence for dia- and paramagnetic domains was the NMR experiment on silver by Condon and Walstedt,[9] where the free induction signal was observed in a single crystal slab at $T=1.4$ K, as H was finely tuned near $H=9$ T. The domains were revealed by the splitting of the NMR line due to two coexisting in-

ductions in the sample, and some basic predictions of the theory were thereby confirmed: the presence of domains within $\delta H \approx \Delta B$ (for $n \approx 1$) and the approximately linear variation of their volume fractions on varying H. Also, the distinct doublet signal showed that the volume for domain-walls (with continuous field distribution) is relatively small. (For domains in Ag see also Ref. 10.)

For the experimental study of Condon domains, beryllium is particularly attractive, since the dHvA frequencies F for $\boldsymbol{H}\|[0001]$ are low, insuring a comfortably large dHvA period of ≈ 41 G already at $H=2$ T. Moreover, domains have been indicated, *in the first place*, precisely in beryllium, on the basis of the particular shape of various dHvA oscillations (like that of magnetization,[1,11,12] magnetoresistance,[13] thermopower[14]). However, the NMR study of Be was not conclusive,[9] since '' . . . the nuclear thermalization time of $\sim 1/2$ h and the inherent quadrupole splitting made the data collection and interpretation difficult.''

Muon spin rotation (μSR) gives, like NMR, *spectroscopic* information on B, but the absence of both quadrupole broadening ($S_\mu = 1/2$) and skin effect is, in this case, an advantage of the muon method. We report here on μSR experiments performed on Be single crystals in fields up to $H=3$ T, at He temperatures down to $T=0.1$ K. For testing various predictions of the theory, Be offers the possibility of an easy variation of the key parameter $\chi_a(B)$: the two nearly equal dHvA frequencies F_h, F_w for $\boldsymbol{H}\|[0001]$ lead to a beat in χ, with $\chi_a^{\max}/\chi_a^{\min} \approx 3$.

By detecting the periodic formation of domains in the wide range $H=1$–3 T of the applied field, the observed behavior of the induction gap ΔB and of the differential susceptibility in the uniform phase, as functions of χ_a, could be compared to theoretical predictions. On tuning H at fixed temperature and, alternatively, varying T at a given field, the possibility of overheating-undercooling at the phase transitions was investigated.

After recapitulating the required basic relations in Sec. II, the experimental results are described and compared to the theory in Secs. III–V. Part of the results have previously been presented as short communications.[15,16]

II. BASIC FORMULAS

A. Magnetic interaction and discontinuity of B

Under the conditions of the dHvA effect, the longitudinal (parallel to the external field $\boldsymbol{H}$) component M of the sample magnetization $\boldsymbol{M}$ is[2]

$$M = -M_1 \sin(2\pi F/B + \phi) + \sum_{p=2}^{\infty} -M_p \sin(2\pi pF/B + \phi_p), \tag{3}$$

giving the susceptibility $\chi = \partial M/\partial B$ in the form

$$\chi = \chi_1 \cos(2\pi F/B + \phi) + \sum_{p=2}^{\infty} \chi_p \cos(2\pi pF/B + \phi_p). \tag{4}$$

The dHvA frequency $F = \hbar c \mathcal{A}_{\text{ext}}/2\pi e$ is determined by the extremal cross section $\mathcal{A}_{\text{ext}}$ of the Fermi surface normal to $\boldsymbol{H}$; the amplitudes $\chi_p \approx (2\pi pF/B^2) M_p$ depend on T, B and on the Fermi surface parameters. For the amplitude of the first harmonic the Lifshitz-Kosevich (LK) formula gives[17,2]

$$\chi_1(B,T;x_D,m^*,\ldots) = \frac{e^2}{4\pi^4 mc^2} \mathcal{A}_{\text{ext}}^2 \left(\frac{2\pi}{|\mathcal{A}''|}\right)^{1/2} \times \frac{m}{m^*} \left(\frac{\hbar c}{eB}\right)^{3/2} G_s R(u,v), \tag{5}$$

where m^* is the cyclotron mass, $\mathcal{A}'' = \partial^2 \mathcal{A}_{\text{ext}}/\partial k_z^2$ is the derivative along the direction of $\boldsymbol{H}$, and the ''reduction factor'' R

$$R_1 \equiv R(u,v) = \{u/\sinh(u)\}\exp(-v); \quad \text{with } u = 2\pi^2 kT/\hbar\omega_c; \quad v = 2\pi^2 k x_D/\hbar\omega_c \tag{6}$$

is due to the finite temperature T and to electron scattering ($x_D = \hbar/2\pi k\tau$ is the Dingle temperature with relaxation time τ), $\omega_c = eB/m^*c$ is the cyclotron frequency; the factor $G_s = \cos(\pi g m^*/2m)$ accounts for electrons with opposite spins ($g \approx 2$). For M_p, χ_p one has $M_p/M_1 = \chi_p/(p\chi_1) = [R(pu,pv)G_s(pm^*)]/[R(u,v)G_s(m^*)]p^{-3/2}$. When more than one $\mathcal{A}_{\text{ext}}$ normal to $\boldsymbol{H}$ exist, as for Be with $\boldsymbol{H}\|[0001]$, the contributions are added.

These formulas contain the *average* magnetic field inside a cyclotron radius $r_c(B) \approx 10^{-3}$–10^{-4} cm, i.e., the induction B. Since in metals the average distance $r_e \sim 10^{-8}$ cm between electrons is, except for very high fields, much smaller than r_c, the orbits strongly overlap. Therefore, apart from their electrostatic interaction, electrons on Landau levels interact via the magnetization they create,[2] and this self-consistency in the dHvA effect leads to the instability discussed below. Two remarks concerning Eqs. (3)–(5):

(1) M_p and χ_p contain a factor $R_p = R(pu,pv)$, so that for $u,v > 1$ second and higher harmonics ($p \geqslant 2$) in Eqs. (3) and (4) can be neglected, leaving only M_1 and χ_1. This *first harmonic approximation* is a high-temperature–low-field approximation within the dHvA regime;

(2) M and χ are periodic in $(1/B)$ but, within a few dHvA cycles near a given $B_0 \ll F$, they are *approximately* also periodic in the variable B,

$$\chi \approx \chi_1 \cos\{2\pi(B-B_0)/\Delta H\},$$

$$M = M_1 \sin\{2\pi(B-B_0)/\Delta H\}, \tag{7}$$

where we chose B_0 to be at a ''paramagnetic'' zero of $M(B)$, $M(B_0)=0$ and $\chi(B_0)=\chi_1$, and $\Delta H = B_0^2/F$ is the ''dHvA period.'' [The above choice of B_0 for the Taylor expansion in Eq.(4) is the simplest, though B_0 may actually not occur as a local value in the crystal.]

Unstable sections in the H,B diagram arise if the amplitude $4\pi M_1$ of the oscillation in $H(B) = B - 4\pi M(B)$ is not small compared to its period ΔH. Consider first a thin rod parallel to $\boldsymbol{H}$ and, for simplicity, sinusoidal dHvA oscillations. If χ_1 is sufficiently large,

$$a(T,B) \equiv 4\pi\chi_1 > 1, \tag{8}$$

the situation is shown in Fig. 1. For a given B, the field H is at the intersection of the straight line, drawn parallel to $y = B$ through the point $4\pi M(B)$, with the B axis. At the

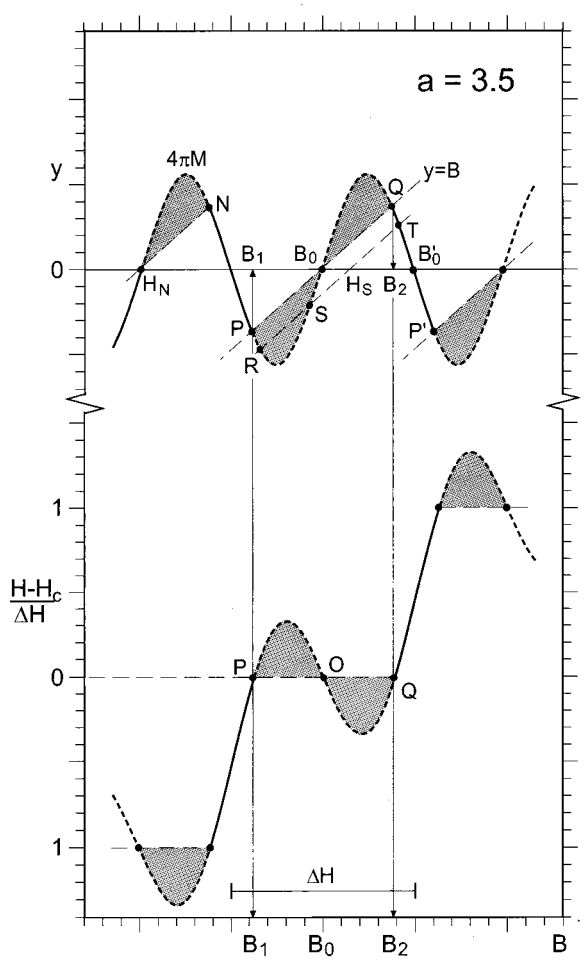

FIG. 1. Magnetization $4\pi M$ and applied field H vs induction B for a long thin crystal oriented along $\boldsymbol{H}$, with $a=4\pi(dM/dB)_{\max}=3.5$, Eq. (7). For a given B_S, the straight line with slope 1 through S gives the cut $H_S=B-4\pi M$ on the B axis. Out of the three magnetizations M_R, M_S, and M_T belonging to $H=H_S$, only M_T is thermodynamically stable. The paths enclosing the filled areas are never realized; M and B jump between the states P and Q having the same free energies. For $n>0$, the magnetizations M_P and M_Q coexist at $H=H_c=B_0$ in the domain phase.

point S one finds, besides B_S, also B_R and B_T belonging to the same H_S: $M(H)$ is *three-valued* in a section of each dHvA cycle. The points B_1 and B_2, with equal free energies $-(1/4\pi)\int^H B\,dH$, enclose a *forbidden interval* (B_1,B_2), within which B is unstable. By Eq. (7) the magnetization $M(H)$, given by the implicit relation

$$m=a\sin(h+m);\quad \text{with}\quad m=8\pi^2M/\Delta H,$$
$$h=2\pi(H-B_0)/\Delta H, \tag{9}$$

is nearly sinusoidal for $a\ll 1$, saw-tooth shaped as $a\to 1$ (Shoenberg effect[2]), and three-valued for $a>1$, in which case M and B vary discontinuously with H, ''leaping over'' the sections with differential paramagnetism $\chi>0$ (Fig. 1). On increasing H from H_N to B_0, M varies along a path with $\chi<0$ from M_N to M_P, where $B=B_1$. Any further increase of H leads to the *jumps* $M_P\to M_Q$, $B_1\to B_2$, where the next diamagnetic section begins.

For sufficiently pure crystals at low temperatures $\chi_1\propto B^{-3/2}$ [Eq. (5)], so that $a>1$ can *always* be fulfilled. For sinusoidal oscillations, the jump $\Delta B(\chi_1)$ and $\chi_{\min}=-\chi_1$ in the diamagnetic sections are interrelated, the forbidden interval is symmetric about B_0 and tends, with increasing χ_1, to extend over the entire dHvA period. For $\Delta B=B_2-B_1$ and B_i one has

$$\pi\Delta B/\Delta H=a\sin\{\pi\Delta B/\Delta H\},\quad B_2,B_1=B_0\pm\Delta B/2 \tag{10}$$

[by Fig. 1, or Eq. (9) with $h=0$, $8\pi M=\Delta B$]. The quantity $\Delta B=\Delta B(B,T)$, predicted by Eqs. (5) and (10), can be compared with the experiment (Sec. II E and Sec. IV). For $\Delta B(a)$, increasing monotonically from $\Delta B(1)=0$, a series expansion gives

$$\Delta B/\Delta H\approx 1-1/(a+1)\quad \text{for}\quad a\gg 1. \tag{11}$$

In this case only B's in the vicinity of B_0', the diamagnetic ($\chi<0$) zeros of $M(B)$, are realized, $B(H)$ consists of nearly horizontal lines connected with vertical jumps.[13]

B. Condon domains

The additional requirement of flux conservation leads, for a multivalued $M(H)$, to the coexistence of two phases. For a disk (ideally an oblate ellipsoid) oriented *normal* to the external field $\boldsymbol{H}$, the boundary condition for a *uniform* state is

$$B=(H-4\pi nM)+4\pi M,\quad M=M(B), \tag{12}$$

where n is the demagnetizing factor. For some ranges of H, however, the required B values lie in forbidden intervals (for $B_1<H<B_2$, for example, if $n=1$).

For $H=H_c=B_0$ in Fig. 1, the uniform, flux-conserving state is O ($B=B_0$, $M=0$). But this state, unstable for the rod discussed in Sec. II A, will not occur in the disk either, since a *nonuniform* flux-conserving state with lower free energy exists:[1] with the sample split up (Fig. 2) into thin plates (of width $d/2$) directed along $\boldsymbol{H}$, magnetized alternatingly parallel ($M=M_Q>0$) and opposite ($M=M_P<0$) to it, the sample average being $\overline{M}=0$. The internal H-field (in a depth $l\gg d$ from the surface) is $H_i=H-4\pi n\overline{M}=H_c$, consistent with the local values M_P,M_Q, and the *mean flux* $\overline{B}=H_c+4\pi\overline{M}$ satisfies the boundary condition.

For $|H-H_c|\leqslant 4\pi nM_Q$ the domain phase is the stable one, H_i stays ''pinned'' at H_c, at which M_P and M_Q (or $B_{1,2}=H_i+4\pi M_{P,Q}$) coexist. What changes with H is the *ratio* of diamagnetic (M_P) to paramagnetic (M_Q) regions, ''adjusting'' $\overline{M}(H)$ so as to insure $H_i=H_c$,

$$\overline{M}=(H-H_c)/4\pi n,$$
$$\text{for}\quad H_1\equiv H_c+4\pi nM_P\leqslant H\leqslant H_c+4\pi nM_Q\equiv H_2. \tag{13}$$

Figures 3(a) and 3(b) show $B(H)$ within a dHvA cycle for different $a=4\pi\chi_1$ and n (first harmonic model). On lowering H from H_c, the diamagnetic ($M=M_P$) domains grow, until at $H=H_1$ one has $B=B_1$ everywhere, and the state remains uniform with B described by Eq. (12). By increasing H from H_c, the paramagnetic ($M=M_Q$) domains grow, un-

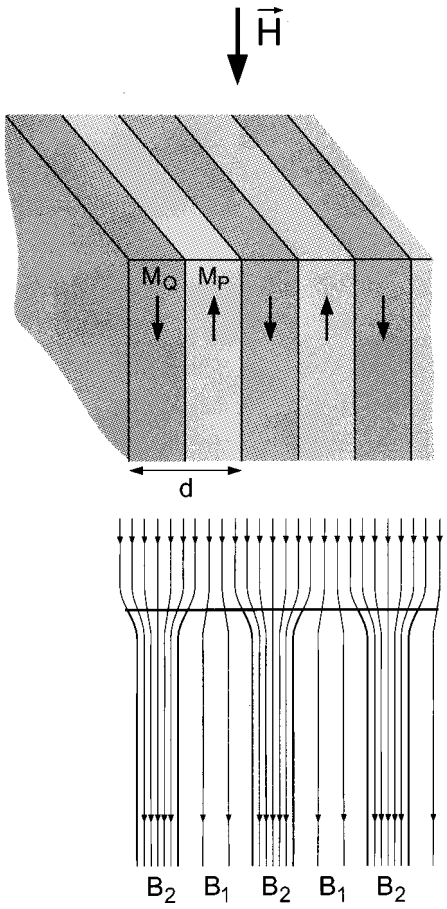

FIG. 2. Condon domains in a plate oriented normal to $\boldsymbol{H}$ (schematic). (a) Planar structure of alternating diamagnetic and paramagnetic regions with period d, for equal volume fractions. The magnetization is either $M=M_Q$ or $M=M_P=-|M_Q|$ (see Fig. 1); (b) induction $\boldsymbol{B}$ inside the sample and at the surface.

til B equals B_2 all over the sample at $H=H_2$. With the volume fraction α_p of paramagnetic domains one has

$$\overline{M}=(1-\alpha_p)M_P+\alpha_p M_Q; \quad \alpha_p=(H-H_1)/(H_2-H_1), \tag{14}$$

and

$$\overline{B}=H_c+4\pi\overline{M}=H/n+H_c(1-1/n), \tag{15}$$

showing that in the domain section $d\overline{M}/d\overline{B}=1/4\pi$ and $d\overline{B}/dH=1/n$. The interval

$$\delta H\equiv H_2-H_1=4\pi n(M_Q-M_P)=n\Delta B \tag{16}$$

is, for a sinusoidal $M(B)$, symmetrical about H_c. Clearly, $\Delta B(a)\to\Delta H$ with increasing a [Eq. (11)], and $\delta H(a,n)$ diminishes with decreasing a and n. One also sees that, besides the exact linearity of $\overline{B}(H)$ within the domain section, $B(H)$ in the *uniform* sections is for $a\gtrsim 3$ *approximately* also linear, $B-B_0'\approx\overline{\mu}(H-B_0')$. This follows from $4\pi M\approx -a(B-B_0')$ for $a\gg 1$, since then the uniform B-range reduces to the vicinity of B_0'. In this case $dB/dH=\mu$ in the uniform phase is, by Fig. 3(a) and Eq. (16), nearly equal to the average

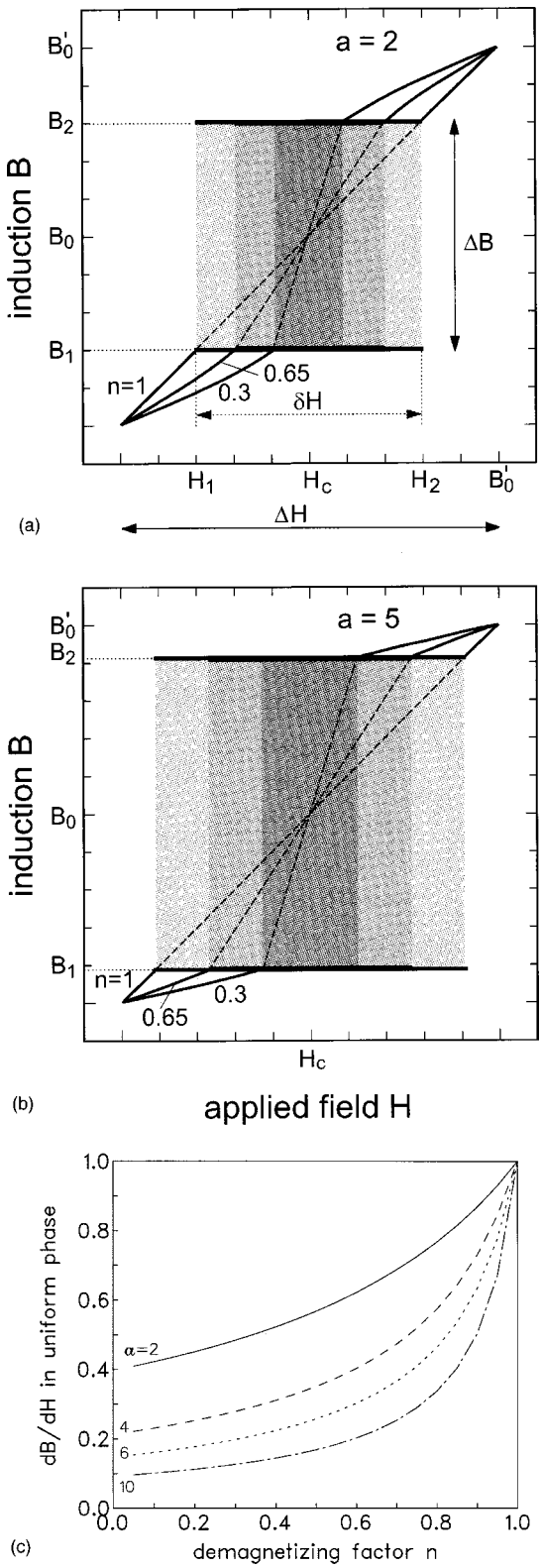

FIG. 3. (a) and (b) $B(H)$ diagrams for different values of $a=4\pi\chi_1$ and n (solid lines). Shadowed areas are domain sections with coexisting $B=B_1$ and $B=B_2$ regions. The interval δH (indicated only for $n=1$) diminishes with decreasing a and n; dashed lines show the sample average $\overline{B}$. (The notation is that of Fig. 1.) (c) Average differential permeability $\overline{\mu}(a;n)$ in the uniform phase.

$$\overline{dB/dH} \equiv \bar{\mu} = (\Delta H - \Delta B)/(\Delta H - n\Delta B) \tag{17}$$

plotted in Fig. 3(c). [For $a<3$ the domain section δH is narrow and the nonlinearity of $B(H)$, visible in Fig. 3(a), may become observable, see Sec. IV A.] By Eq. (12)

$$4\pi\chi = (1-1/\mu)/(1-n), \tag{18}$$

giving $1/\bar{\mu} \approx 1 + a(1-n)$ for $a \gg 1$. Apart from the infinite disk ($n=1$) where $\mu = \bar{\mu} = 1$ irrespective of a, for $n<1$ the uniform sections show *differential diamagnetism*, $\bar{\mu}<1$. The decreasing slope $\bar{\mu}$ of the lines $B(H)$ with increasing a and $(1-n)$ is seen in Figs. 3(a)–3(c).

C. Domain form

No data are available on the morphology of Condon domains, the planar structure, varying only along one direction as in Fig. 2, is just the simplest assumption. Predictions on the period d and on the size and magnetic structure $\boldsymbol{M}(\boldsymbol{r})$ of the ''wall'' regions exist[6,18–20] but have not as yet been experimentally confirmed.

The period d is determined[17,2] by the formation energy of the planar interfaces and the energy of bending these planes, as they emerge at the sample surface. This gives

$$d \sim \sqrt{Lw} \tag{19}$$

provided $d \ll L$, where L is the thickness of the plate and w the width of the wall region which [except for $\Delta B \ll \Delta H$ (Ref. 18)] should be of the order of $r_c \sim 10^{-4}$ cm for $H \sim 1$ T.

The prediction $w/d \sim \sqrt{w/L} \ll 1$ for $L \sim 0.1$ cm thick samples is confirmed by the earlier NMR results on Ag (Ref. 9) and also by the present μSR data for Be, insofar as two distinct frequencies in the spectra are evidence that the volume fractions for the essentially homogeneous ''in-domain'' regions dominate, with small volume left for boundaries. For the study of small-scale variations of $\boldsymbol{B}(\boldsymbol{r})$, subject of several model calculations,[6,18–20] the *shape* of the spectral lines has to be known in a higher than present-day accuracy.

D. Fermi-surface parameters of beryllium, beat for $H \| [0001]$

The electron part of the Fermi surface[21] of Be consists of two equivalent cigar-like ellipsoids oriented along the [0001] direction and slightly pinched in the middle, forming a ''waist'' and two symmetrically placed ''hips.''

The cross sections $\mathcal{A}_{\text{waist}}$ and $\mathcal{A}_{\text{hip}}$ give rise to two frequencies $F_w = 942.2 \pm 0.3$ T and $F_h = 970.9 \pm 0.5$ T, causing a *beat* in $\chi(B)$ with the frequency $F_h - F_w = 28.7 \pm 0.2$ T.[22] The antinode and node values $\chi_1^{(h)}$ and $\chi_1^{(l)}$ of the amplitude are $\chi_1^{(h,l)} = 2(2 \pm 0.94)\chi_{1,\text{hip}}$, in view of the two hips and the ≈ 3 percent thinner waist for each ellipsoids; here $\chi_{1,\text{hip}}$ is given by Eq. (5) with $\mathcal{A}_{\text{ext}} = \mathcal{A}_{\text{hip}}$. The beat cycle of χ_1 comprises ≈ 33 dHvA periods, the measured susceptibility $\chi(B)$ (Ref. 11) is reproduced in Fig. 4. Since both $\Delta B(a)$ in the domain phase and $\mu(B;a)$ for the uniform state depend on χ_1, the ''natural'' variation of this parameter along the beat cycle allows one a thorough check of the theory (Sec. III).

The quoted values of F, with $m^* = 0.17m$ and $|\mathcal{A}''| \approx 0.25$ for this geometry, lead to the phase diagrams discussed in the next section. Note that the small m^* and the little curvature $|\mathcal{A}''|$ along [0001] result in a relatively large dHvA amplitude even at the not too low temperatures of 1–2 K and for magnetic fields not higher than 2–3 T.

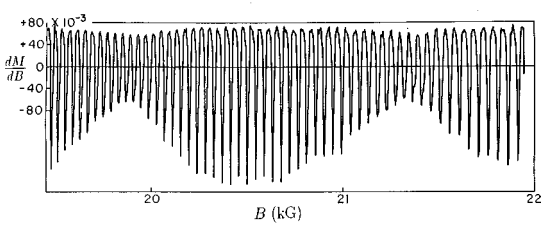

FIG. 4. Beating magnetic susceptibility $\chi(B)$ of beryllium at $T = 1.4$ K for $\boldsymbol{B} \| [0001]$, measured on a cubical crystal.[11] The asymmetric shape is due to the missing of paramagnetic sections with $\chi > 1/4\pi$, where Eq. (15) is valid.

E. The phase transition

While the jump of B for a long thin cylinder is obviously a transition of first order (''boiling''), the order of the uniform $\leftrightarrow$ domain transition depends on where the phase boundary is crossed and in which direction.

The ''envelope'' line $a(B,T) = 4\pi\chi_1 = 1$ in the (B,T) plane, shown in Fig. 5(a), separates two regions. Above it $a<1$ and the state is uniform, below it one has $a>1$ and domain ''strips'' arise, parallel to the T axis and centered along the inductions $B = B_{0i}$ (the paramagnetic zeros of M) in each dHvA cycle, the uniform state reappears between the strips. The width $\Delta B(a[T])$ of each strip decreases with increasing T, becoming zero at T_0, where $a(B_0, T_0) = 1$ for the field in question. [Since, by Eqs. (5) and (6), $da/dT < 0$, Eq. (10) for $\Delta B(a)$ implies that $\Delta B(T)$ is monotonically decreasing.] The envelope $a(B,T) = 1$ is *not* a phase boundary, it just spans the ''critical'' points, i.e., the high-temperature ends, of the narrowing domain regions. For Be, the small scale strip structure of the actual phase boundary is modulated by the ''medium scale'' variation due to the beating of χ, and the envelope in Fig. 5(a) is seen to oscillate between the ''higher'' and ''lower'' limiting envelopes $4\pi\chi_1^{(h,l)}(B,T;x_D) = 1$, corresponding to the beat maxima and minima. In Fig. 5(b) only these ''limiting'' envelopes are plotted, for different Dingle temperatures.

The envelope curves in Figs. 5(a) and 5(b) were calculated by Eq. (5), using the Fermi-surface data of Sec. II D (the spin factor $G = 0.87$ was neglected). For the field range below *both* solid and dashed curves (for a given x_D), there is a domain strip in each dHvA period. For fields *to the right* of a given dashed curve, the envelope $a(B,T) = 1$ drops, in each beat cycle, from the $4\pi\chi_1^{(h)} = 1$ line down to the B-axis, excluding domain strips near the beat nodes.

As will be shown in Sec. IV, we observed domains in a much more extended region of the B,T plane than the curves in Fig. 5(b) predict. Here we note only that this is *not* due to an unjustified neglect of higher harmonics in the LK formula. With $m^*/m = 0.17$, the arguments in the factors R_p [Eqs. (5) and (6)] are $u = 2.50T/B$ and $v = 2.50x_D/B$ (B in tesla, T in K). Thus, with $x_D = 2$ K (even lower than 2.6 K cited in Ref. 12) one has, at e.g. $T = 0.1$ K and $B = 2.5$ T, the

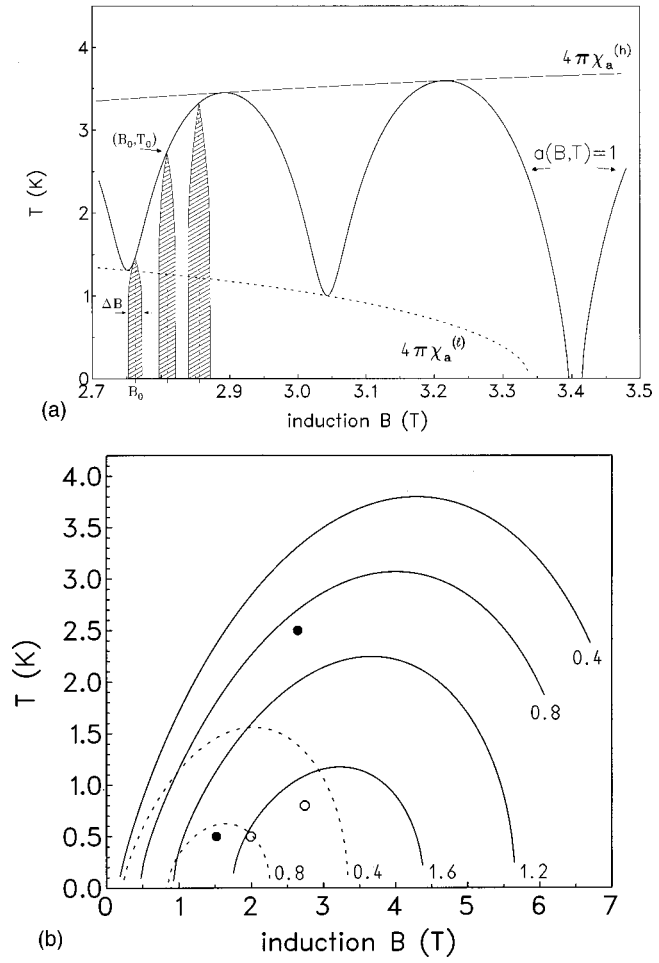

FIG. 5. Calculated phase diagrams for Be, $\boldsymbol{H}||c$ axis [Eqs. (5) and (8)]. (a) Section of the oscillating envelope $a(B,T)=1$ for $x_D=0.4$ K. The beat cycle in reality contains $\approx$33 dHvA periods but here, for visibility, only 3 domain strips (shadowed) are schematically drawn, the width of the strips and that of the dHvA period are magnified by a factor of $\approx$6. The envelope $a(B,T)=1$ is discontinuous above $B\approx 3.39$ T (for this value of x_D); for higher fields the strips near the beat minima disappear. (b) Higher and lower envelopes $4\pi\chi_a^{(h,l)}=1$ (solid and dashed curves) for different Dingle temperatures x_D (in K). For $x_D\geqslant 0.87$ K no strips should appear at the beat nodes, and for $x_D>1.78$ K not even at the beat maxima. The experimental points for two beat antinodes (●) and beat nodes (○) show *observed* domain phases for the sample with $x_D\approx 2.6$ K.

amplitudes of the first few harmonics in Eq. (4) decreasing like $\chi_1:\chi_2:\chi_3=1:0.053:0.0004$, already the 2nd harmonic is fairly small.

On crossing the phase boundary along a vertical line $B=B_0$, where the domains have equal volume fractions, the transition occurs at $a(B_0,T_0)=1$. By Eq. (9), for $T_0-T\ll T_0$ one has

$$\Delta B/\Delta H\approx C\sqrt{1-T/T_0};\quad T<T_0,$$

$$C=[(6T_0|\partial a/\partial T|_{H_0,T_0})/\pi^2]^{1/2}, \tag{20}$$

(see also Ref. 7), as expected for a second order transition at the critical point (B_0,T_0). The constant, by Eqs. (5) and (6), has the value

$$C=\sqrt{6(u_0\coth u_0-1)}/\pi;\quad u_0=2\pi^2kT_0/\hbar\omega_c. \tag{21}$$

The treatment of the ''vertical'' transition at a constant $B\neq B_0$ [with $a(B,T_{tr})>1$ at the transition temperature T_{tr}] is more complex.[8]

In traversing the boundaries horizontally by variation of B at a constant $T=T_1$, two first order ''electronic topological transitions'' (Ref. 5) per dHvA cycle occur. In this case regions with a *finite* induction difference ΔB are formed, even if one of the volume fractions starts continuously from zero. In the NMR study of Ag (Ref. 9) supercooling was observed: no domains were formed when the sample had been cooled down to $T_1=2.2$ K, though domains were observed when the same T_1 was reached by heating the crystal.

F. The evaluation of μSR spectra

In the ''transverse field'' muon-spin-rotation (μSR) method[23] spin-polarized μ^+ particles are implanted in the sample and, on applying a homogeneous magnetic field $\boldsymbol{H}$, the free precession of their spin about the local field $\boldsymbol{B}$ is monitored. By counting the number $N(\boldsymbol{\Omega},t)dt$ of the positrons, emitted by the μ^+ decay into a given solid angle $\boldsymbol{\Omega}$ at a time $(t,t+dt)$ after implantation, the movement of the muon spin $\boldsymbol{S}_\mu$ is detected, since in the parity nonconserving $\mu^+\rightarrow e^+ +\nu_e+\overline{\nu}_\mu$ decay the momentum of the e^+ points preferentially into the *instantaneous direction* of $\boldsymbol{S}_\mu$. The counting rate $N_k(t)$ for a positron detector k within the plane of the spin precession has, thereby, an *oscillating* component. By histogramming a large number of individual μ^+ decays the ensemble average for all muons, randomly stopped within the sample, is obtained. The Fourier analysis of $N_k(t)$ gives the distribution of the precession frequencies $\omega=\gamma_\mu B$, i.e., that of the local fields ($\gamma_\mu=2\pi\times 135.5388$ MHz T^{-1} is the gyromagnetic ratio of the muon). Free of quadrupolar line broadening ($S_\mu=1/2$) and of limitations due to skin effect, the μSR method is very advantageous in the present context, as pointed out first in Ref. 24.

For two detectors, left (l) and right (r) of the sample in a plane normal to $\boldsymbol{B}$, we have

$$N_k(t)=N_{0k}e^{-t/\tau_\mu}\{1+A_kP_k(t)\}+b_k;\quad k=l,r, \tag{22}$$

where the exponential decay with the μ-lifetime $\tau_\mu=2.197$ μs determines the time window for observation, b_k is an accidental background. Basic to the method are the ''maximum positron asymmetries'' A_k, arising from the anisotropy of the e^+ emission. Averaged over all e^+ energies one has $A_k=1/3$, but this value is reduced because of the finite spatial and time resolutions. For transverse-field μSR the initial μ^+ polarization is (ideally) perpendicular to $\boldsymbol{B}$, and P_k is the *time dependent muon polarization function*, having the form

$$P_k(t)=\int dB'D(B';B)\cos(\gamma_\mu B't+\phi_k),\quad k=l,r, \tag{23}$$

where ϕ_l, $\phi_r\approx\phi_l+\pi$ are the phases at $t=0$ at the corresponding detectors, and $D(B';B)$ is the (normalized) distribution of the field magnitude B' at the μ^+ sites for a mean value B.

In the uniform state of a nonmagnetic metal, $D(B';B)$ is narrowly centered about $B=B(H)$, and $P_k(t)$ describes a damped oscillation with frequency $\omega=\gamma_\mu B$. The damping is due to small random spatial fluctuations of the local fields B', which broaden D and lead to a ''destructive'' dephasing of the precession of individual muons. (In the present case, fluctuations arise from the randomly oriented *nuclear* magnetic moments.) Due to the fast diffusion of μ^+ in the beryllium lattice at the present temperature range, $P_k(t)$ is *exponentially* decreasing,

$$P_k(t;H)=e^{-\lambda t}\cos(\gamma_\mu Bt+\phi_k); \quad B=B(H), \qquad (24)$$

corresponding to a motional-narrowed, Lorentzian $D(B';B)=(\lambda/\pi)/\{(B'-B)^2+\lambda^2\}$. From the data for $H<0.6$ T near $T=1$ K the value $\lambda=\lambda_0\lesssim 0.05\times 10^6$ s^{-1} was deduced, consistent with random nuclear dipole fields of $\lesssim 1$ G at the interstitial μ^+ sites.

The nonellipsoidal shape of the sample brings additional inhomogeneity in B, and this, as expected on the basis of the measured values of χ in the *uniform* phase (Sec. IV), leads to an observed, steady increase of λ with increasing H, up to $\approx 0.3-0.4\times 10^6$ s^{-1} near $H=3$ T.

For ''ideal'' Condon domains, with homogeneous intradomain magnetizations and negligibly small wall regions, *two* oscillatory terms are expected

$$P_k(t)=\sum_{j=1,2} a_H^{(j)} e^{-\lambda^{(j)}t}\cos(\gamma_\mu B_j t+\phi_k), \qquad (25)$$

where the frequencies $\gamma_\mu B_1$ and $\gamma_\mu B_2$, corresponding to the para- and diamagnetic regions, *do not vary with H*, unlike in Eq. (24). For randomly distributed μ^+ positions, the *amplitudes* $a^{(1)}(H)$ and $a^{(2)}(H)$ are *identical* with the volume fractions $\alpha_p(H)$ and $(1-\alpha_p)$ of Eq. (14).

In reality, besides the two peaks at B_1 and B_2, the distribution $D(B';B)$ has also a contribution from domain-wall regions where $\boldsymbol{M}$ is neither parallel nor opposite to $\boldsymbol{H}$. Thus, even if M is constant within the bulk of a domain (which has been questioned[20]), D is not entirely ''empty'' between its two peaks. An empirical way to take this into account is using λ's as adjustable parameters in Eq. (25); this will be done in Sec. III.

III. EXPERIMENT

The experiments were performed at the low temperature μSR facility, LTF, of the Paul Scherrer Institute, Villigen. The applied magnetic field $\boldsymbol{H}$, oriented along the direction of the incident ''surface'' μ^+ beam (of momentum 28 MeV/c) was normal to the Be single crystal plate, the initial muon polarization had an angle of $\approx 50°$ with $\boldsymbol{H}$. At the two detectors placed left and right of the sample in the precession plane, typically $\approx 10^7$ μ^+ decays for each H,T points were detected. ''On the spot'' measurements of the thermopower oscillations were used to test the setup (field homogeneity, orientation).

The two samples (residual resistance ratio $R_{300}/R_{4.2}\approx 300$) were cut from a single crystal rod, with the axis [0001] normal to the plate. The ''thick'' Be-1 and the ''thin'' Be-2 samples had dimensions of $0.9\times 1\times 0.18$ cm^3 and $0.9\times 1.4\times 0.09$ cm^3. The mean penetration length of the μ^+ beam, incident on sample, is $\approx 0.06\pm 0.01$ cm, thus practically all muons are expected to stop even in the thin Be-2 sample.

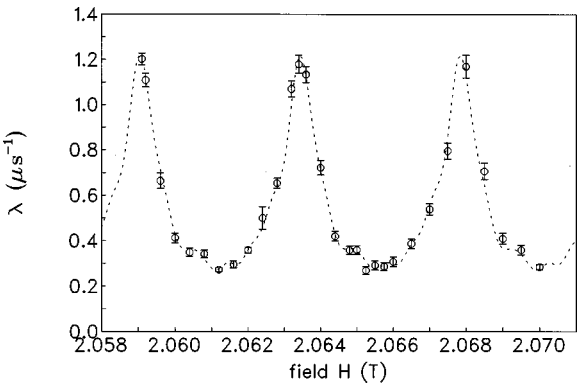

FIG. 6. Exponential damping rate λ at $T=0.5$ K as a function of H, inferred via Eq. (24). The periodic sharp rise of λ (i.e., of the linewidth $\Delta\omega=2\lambda$ in frequency space at $\omega=\gamma_\mu B$) indicates a split line, interpreted as ''broad'' by Eq. (24). The dotted curve is best fit to the data by a truncated Fourier series, the period of which, 44.0 G, turns out to be the dHvA period $\Delta H=B_0^2/F=43.9$ G (for $B_0=2.0645$ T).

At this orientation the dHvA period is $\Delta H=B_0^2/F\approx 64$ G for $B=2.5$ T (with $F_h=970.9$ T). Thus, for a reasonable mapping of the domain range within a dHvA cycle, a B scan in steps of some G is required, with a corresponding homogeneity and stability of the applied field. The field homogeneity in the sample at low fields was found to be $\delta B<1$ G, and the deviations during a typical measuring time of ≈ 1 h remained also in this limit. In a first series of experiments the scans were made by steps of 7 G, in the following the mesh was reduced to 2 G or less.

IV. RESULTS AND DISCUSSION

A. Domain phase and diamagnetism of the uniform state

In this section, field scans near some selected ''reference values'' $B_0>1.5$ T are presented, for temperatures $T=0.1-0.5$ K. At this range of the B,T plane, the presence of domains in Be is visible as a μSR doublet. For lower fields, with decreasing $\Delta H\propto B_0^2$, the lines of the doublet merge together, but domain formation still can be detected by the periodic *broadening* of the spectrum line, down to $B_0\approx 0.9$ T. The physical parameters, like the domain splitting $\Delta B=B_2-B_1$ and permeability $\mu\equiv dB/dH$ of the uniform phase, show a strong variation, as the reference field B_0 moves along a *beat cycle* of $\chi(B)$.

Results of a field run at a *beat antinode* of χ on the ''thick'' Be-1 sample are seen in Fig. 6, where the line width λ [Eq. (24)] is plotted against H. [In fact, the one-frequency fit by Eq. (24) is adequate only for the uniform state but, at first, we neglect this ''detail'' and interpret the data on the entire field range by the same equation. This amounts to considering the domain-doublet as a single, broad line, with an effective linewidth proportional to ΔB.]

The oscillatory ''dHvA'' variation of λ in Fig. 6, observed for the first time in μSR spectra, is spectacular. The dotted curve is a best fit by a finite Fourier series $\Sigma_0^n\{a_i\sin(2\pi iH/\Delta)+b_i\cos(2\pi iH/\Delta)\}$, and the period Δ

$=44.0$ G turns out, as expected, to be the dHvA period (for $B_0=2.0645$ T and $F=970.9$ T, one has $\Delta H=B_0^2/F=43.9$ G).

The minima of λ are line widths for the uniform state, while the maxima provide an estimate for ΔB in the domain phase. In using Eq. (24) one would, at first sight, expect only two possible values: $\lambda=\lambda_u$ for the uniform state, and a much larger ''effective'' one (see above), $\lambda=\lambda_d\approx\pi(\gamma_\mu/2\pi)\Delta B$ for the domain section. The (overly simplified) assumption of a single frequency and exponential decay for Eq. (24) leads to the smooth descent from the peak value λ_d to λ_u, as the volume fraction of the minority domains decreases. This explains the continuous variation of $\lambda(H)$ in Fig. 6, but some details, like the minimum (instead of a broad plateau) for the uniform state at λ_u, and the shoulder at $\lambda\approx 0.3\ \mu s^{-1}$, are not completely understood at present.

By Fourier transforming the depolarization function $P_k(t)$, in Figs. 7(a) and 7(b) the power spectra of the spectral lines are plotted for H near the central region of Fig. 6. One sees that the large broadening $\lambda_d=1.2\ \mu s^{-1}$ at $H=20634$ Oe in Fig. 6, obtained via the one-frequency fit by Eq. (24) is, in reality, a well resolved *doublet*, with components at $B_1\approx 20607$ G and $B_2\approx 20643$ G, of approximately equal intensities. (From $\Delta B=36$ G one expects $\lambda=1.5\ \mu s^{-1}$, consistent with λ_d above.) The variation of intensities with decreasing H clearly shows that for $H=20640$ Oe [Fig. 7(a)] the diamagnetic component (at $B_1=20607$ G) is small, for $H=20634$ Oe the dia- and paramagnetic lines become of equal intensity, and for $H=20628$ Oe [Fig. 7(b)] the diamagnetic line dominates.

The $B(H)$ diagram at the same beat maximum $\chi_a\approx\chi_1^{(h)}$, Fig. 8(a), was determined by using Eq. (25) and, when no two frequencies can be resolved, by Eq. (24). The theoretical curve is found by varying the ''amplitude parameter'' a [Eq. (9)] to have a best fit, at the given demagnetizing factor $n=0.775$. (By the tables,[25] the inscribed ellipsoid of the rectangular $10\times 9\times 1.8$ mm^3 Be sample gives $n\approx 0.77\pm 0.02$. Further, the same value for n was inferred from our data with χ_a at the *nodal* region, where the ''uniform'' section in the dHvA cycle is larger and n can more accurately be determined; see below.) The best fit for a is obtained for $a_h=3.64$, where the subscript of $a_h=4\pi\chi_1^{(h)}$ refers to the beat antinode. In the sinusoidal case one has $a=a(\Delta B/\Delta H)$ and the above value of a corresponds, by Eq. (10), to $\Delta B\approx 34$ G or $\Delta B/\Delta H=0.77$. The overall agreement for $B(H)$ in Fig. 8(a) is reasonable, except for a deviation near the high-field ends of the domain ranges. The observed, approximately linear variation of the intensities of the doublet components (volume fractions) for the same domain sections are seen in Fig. 8(b).

The slope $\overline{dB/dH}=\bar{\mu}=0.55\pm 0.1$ in the uniform phase gives [Eq. (18)] $4\pi\overline{dM/dB}=-3.6$, consistent with the first harmonic model requiring $-4\pi\chi_1=-a=-3.64$. [This is not yet a proof for a sinusoidal $M(B)$, since for $a>3$ only a small section of the ''theoretical'' $M(B)$ is observable, as noticed in Sec. II B.] Important is that the experiment provides an *absolute measurement of the dHvA susceptibility* $\chi(B)$ for all physically accessible B values.

On tuning H downwards by half of a beat period, a decreases, and Fig. 9 shows $B(H)$ for $\chi_a=\chi_1^{(l)}$, at the beat

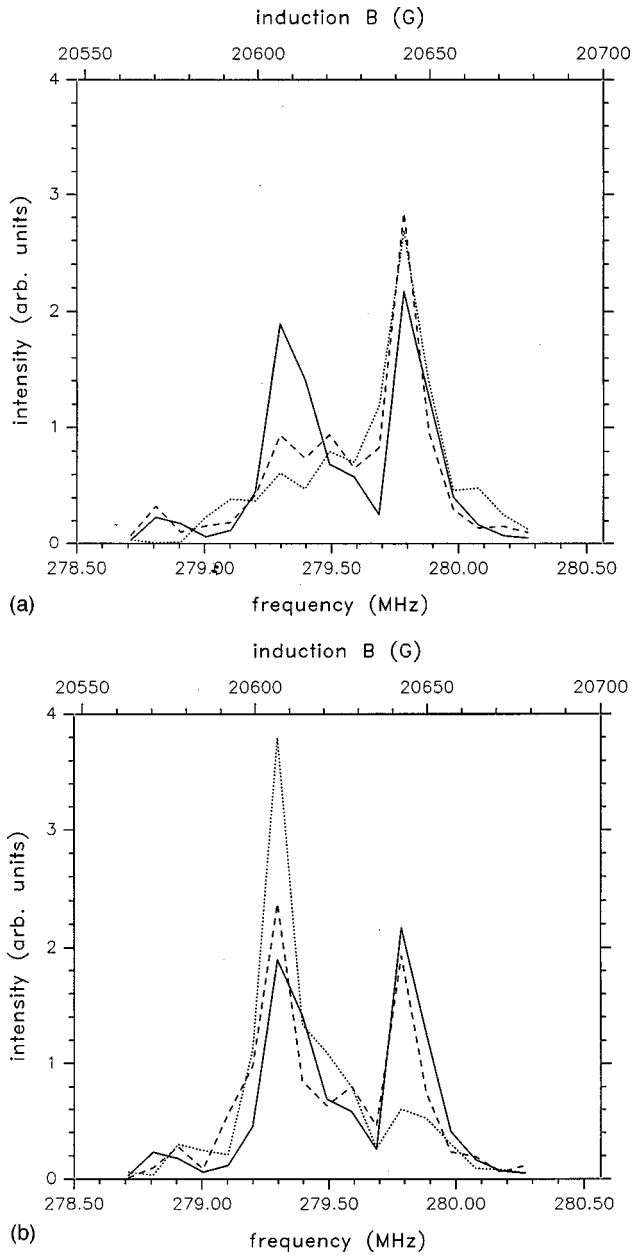

FIG. 7. Doublet splitting of the μSR line at $T=0.5$ K, evidencing of dia- and paramagnetic domains. The applied field varies near a *beat maximum* (Fig. 4). The spectra belong to five subsequent, decreasing values of H, corresponding to the five points about the central maximum in Fig. 6: (a) $H=20640$ (dotted), 20636 (dashed), and 20634 Oe (solid line), and (b) $H=20634$ (solid), 20632 (dashed), and 20628 Oe (dotted line). Note the stable positions ($B_1\approx 20607$ G, $B_2\approx 20643$ G) of the peaks, while the intensity ''flows'' from the upper to the lower line as H decreases. (The area of the doublets is normalized to unity.)

node. The domain-free section is longer, the mean permeability $\bar{\mu}=0.83$ much larger than for the antinode region. Variation of both n and a gives $n=0.775$ and $a_l=4\pi\chi_1^{(l)}=1.25$ as best fit to the data. Here Eq. (18) with $\mu\to\bar{\mu}$ would give $4\pi\chi\approx -0.79$ for the minimum susceptibility, in apparent contradiction with a sinusoidal $M(H)$, since for this value of $(-a)$ no domains should occur at all. However, nonlinearity cannot be neglected for $a\gtrsim 1$ [see Fig. 3(a)]: the

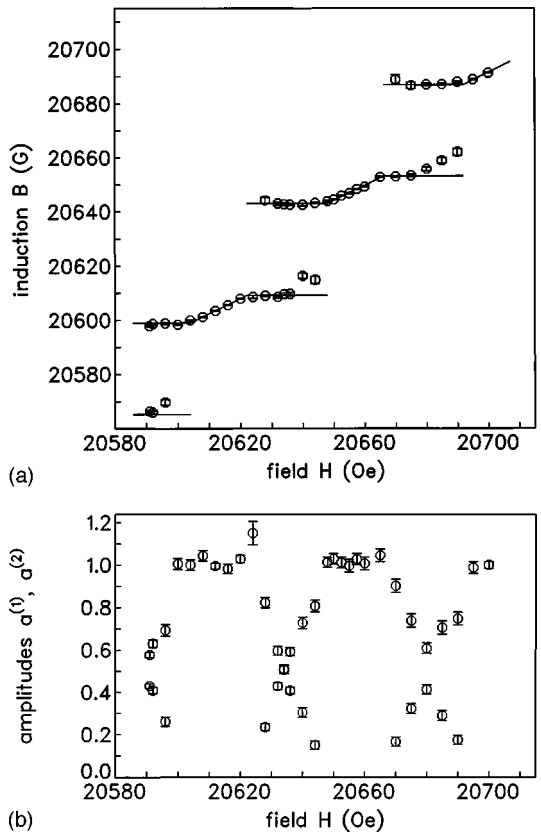

FIG. 8. (a) $B(H)$ diagram at $T=0.5$ K, showing the recurrent doublet structure at a beat maximum (the field range is that of Figs. 6 and 7). The theoretical curve (solid line) is for $a=3.64$ and $n=0.775$. (The nominal H scale has an upwards shift of ≈ 8.7 G with respect to the actual field values.) (b) Normalized line intensities $a^{(j)}$ [Eq. (25)]. For the sections with doublet splitting, $a^{(j)}$'s are the volume fractions of the oppositely magnetized domains, predicted to vary linearly with H.

theory predicts $\mu < \bar{\mu}$ in the middle of the uniform section, reproducing $4\pi\chi(B_0')=-1.25$ for the minimum of χ. [The slight nonlinearity in the theoretical $B(H)$ curve cannot, at the present accuracy, be either unambiguously confirmed or invalidated by the data points.] Our ratio $\chi_1^{(l)}/\chi_1^{(h)}=a_l/a_h=0.34$ is near to the value 0.32, expected for the almost equal two hip and one waist cross sections.

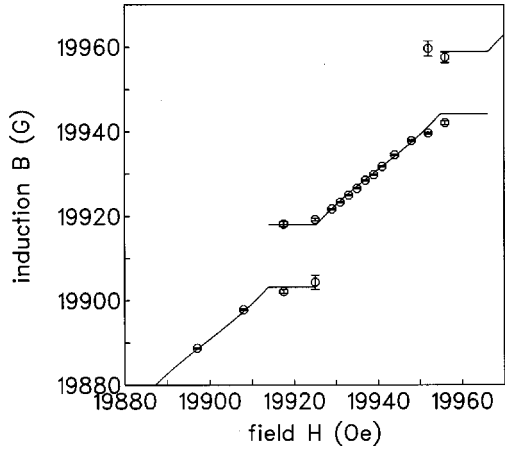

FIG. 9. $B(H)$ diagram at $T=0.5$ K, as in Fig. 8, but for $\chi_a(B)$ at the nearest beat *node* (Fig. 4). The theoretical curve (solid line) is for $a=1.25$ and $n=0.775$.

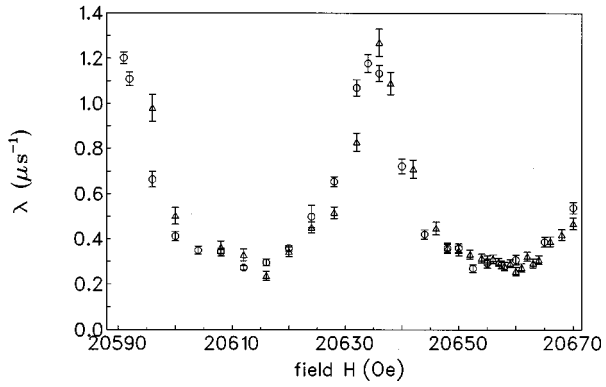

FIG. 10. Comparison of the damping rates $\lambda(H)$ for field scans downwards (○) (Fig. 6) and upwards (△), at $T=0.5$ K. A slight shift of the upwards series towards higher H's (''field-overheating'') is visible.

The data shown in Figs. 6–9 were taken by tuning H downwards. To test reversibility, a series of measurements was also done by *reincreasing* H in the same interval. As seen in Fig. 10, the peak for the ''upwards'' series is slightly shifted for higher H with respect to that measured ''downwards,'' an indication for field ''overheating'' by an amount of $\lesssim 2$ G.

To see the predicted increase of δH and $\bar{\mu}$ for larger n, measurements were also performed on the thinner Be-2 sample with $n=0.88\pm0.02$. While domains, similarly to Figs. 6–9, could be observed via broadening or splitting of the frequency spectra also for Be-2, the quantitative interpretation of the data is more difficult, since the doublet lines are less distinct than for Be-1. For example, Fig. 11 shows $B(H)$ for Be-2 at the same beat maximum as Fig. 8(a) for Be-1, the fit giving in this case $a=2.01$ and $n=0.72$. However, these values are not realistic, since n for Be-2 is certainly larger than for Be-1, and a should be about the same for the plates cut from the same crystal.

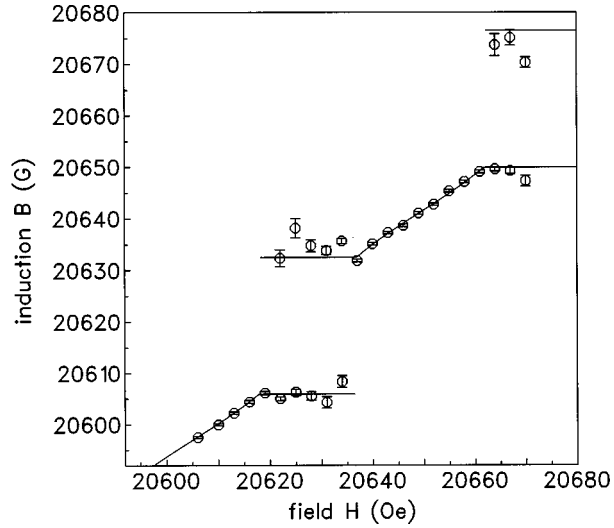

FIG. 11. $B(H)$ diagram as in Fig. 8, but for sample Be-2. The calculated curve is for $n=0.78$ and $a=1.25$.

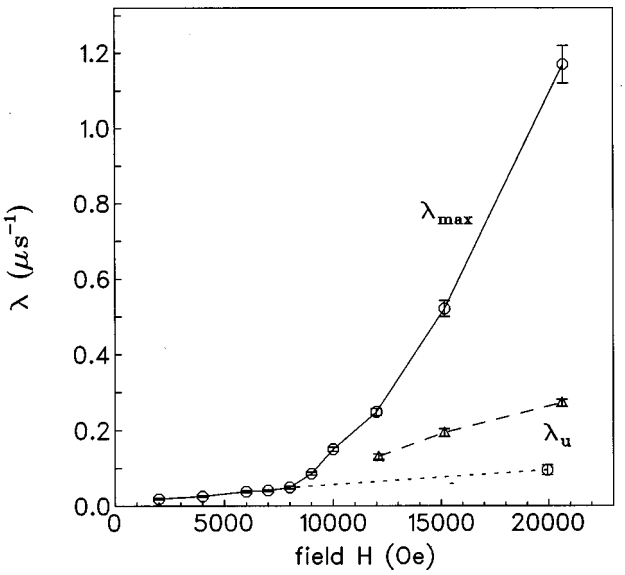

FIG. 12. Damping rate $\lambda(H)$ at $T=0.1$ K for selected phases of the beat and dHvA periods. Solid line: λ in the middle of domain sections near beat antinodes (λ_{max}); dashed and dotted lines: λ for uniform states (λ_u) near beat maxima and minima, respectively. The branch λ_{max} appearing at $H\approx 0.9$ T indicates domain formation from this field upwards. (The points $H>1.2$ T belong to $T=0.5$ K.)

The merging spectral lines for Be-2 may signalize that the volume fraction of the inhomogeneous wall regions is, for the thinner sample, more important. In this case the fit by only two frequencies is obviously less adequate, with the numerical consequence that the deduced values for ΔB and a are systematically too small, as indeed the fit result shows. Thus, in spite of the order-of-magnitude estimate Eq. (19) for $L=0.09$ cm and wall thickness $w\approx 10^{-4}$ cm, giving a ratio as small as $w/d=0.03$, the result for Be-2 may indicate that the actual wall thickness is *considerably larger*. On the other hand, the ''opening'' of the domains in surface layers of thickness $\approx d$ also diminishes the volume fraction of the homogeneous regions. For $w\approx 10^{-4}$ cm, the layers with bent domain walls make up $2d/L\approx 2\sqrt{w/L}\approx 6.7$ and ≈ 4.7 percents of the volume for Be-2 and Be-1, respectively.

B. Reversibility and phase boundaries

On crossing the envelope $a(B,T)=1$ [Fig. 5(a)] along a horizontal ($T=$const) line, the domain structure appears first as the onset of a periodic oscillation of λ (near the envelope curve the domain strips are narrow, $\Delta B \ll \Delta H$, the splitting is difficult to resolve).

In Fig. 12 the variation of λ is seen at fields corresponding to selected positions (''phases'') within the beat and dHvA periods. The data show λ in the ''middle'' of the uniform phase ($\lambda_u, H=B'_{oi}$) both at the beat minima and maxima, and also within the domain strips at 1:1 volume fractions ($\lambda_{max}, H=B_{0i}$). The ''branch'' λ_{max} arises at $H=0.9$ T, indicating the lowest field where domains appear in our μSR spectra. Comparing to the phase diagram [Fig. 5(b)], this would mean $x_D \leqslant 1.2$ K, but x_D in reality is higher (see below). One sees that λ_u in the *uniform* state is different whether measured near a beat antinode or node. This is due to the fact that, for $\chi_1=\chi_1^{(h)}$, the spatial variations of M and B in the nonellipsoidal sample, scaled by M itself, are also larger. (The points for the highest fields were measured at $T=0.5$ K, but λ_{min} varies little for $T<0.5$ K.)

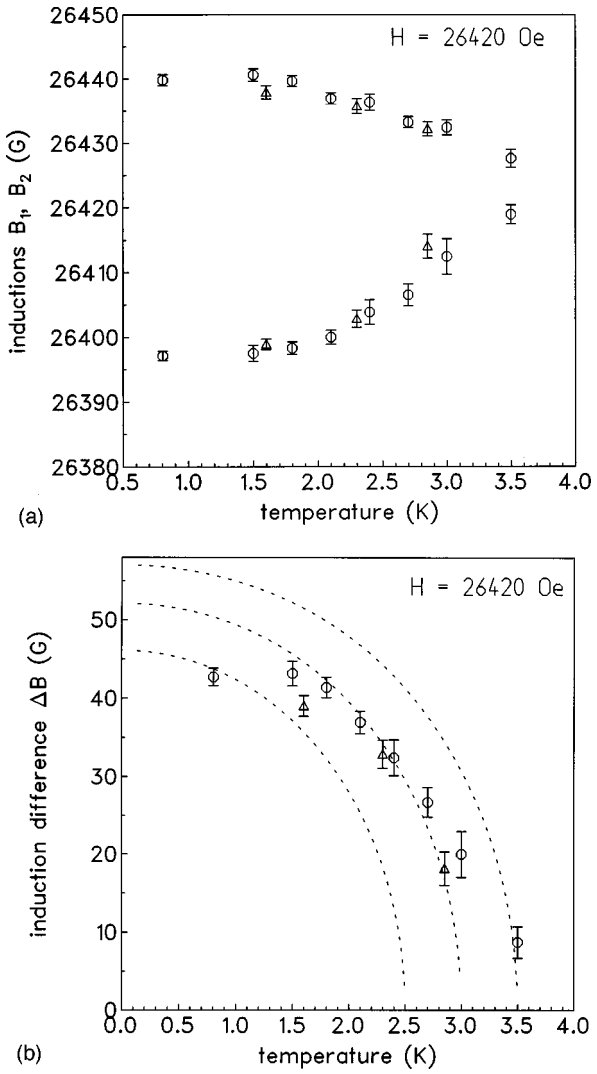

FIG. 13. (a) Domain inductions B_1, B_2 as functions of temperature for Be-1 at $H=26420$ Oe; ○: sample heated; △: sample cooled. For $T>3$ K the resolution of two frequencies is increasingly difficult; (b) the induction difference ΔB as a function of temperature. The dotted lines are predictions of the first harmonic approximation for the transition point at $T_0=2.5,\ 3.0$, or 3.5 K.

Next, the variation of $B_2-B_1=\Delta B$ was studied as a function of T for a field $H=B_0$ in the ''middle'' of the domain section, along the vertical path considered in Sec. II E. Figure 13(a) shows, for $H=26420$ Oe, how the inductions B_1, B_2 converge as T increases. The data for the runs of increasing and decreasing temperatures do not differ significantly within our accuracy of ≈ 0.2 K. In Fig. 13(b) the difference ΔB is plotted, together with the prediction of Eqs. (10), (5), and (21) for different values of the critical point ($T_0=2.5,\ 3.0$, and 3.5 K). Though the drop of ΔB between 1.5–3 K is not far from the expected one for $T_0=3$ K, the transition to the low temperature plateau with decreasing T is significantly sharper as predicted.

The observed deviation from the numerical predictions of the theory is even more important for the phase diagram, Fig. 5(b). In view of the known value ($x_D\approx 2.6$ K) of the Dingle

temperature for our sample,[12] the selected representative data points indicate a much more extended area for the domain phase than expected. Since $B=2.641$ T (filled circle) is at a beat *maximum* of χ_1, the presence of domains at $T_0=2.5$ K would already imply that $x_D<0.9$ K. The data points at the beat *nodes* $B=1.992$ T at $T=0.5$ K and $B=2.739$ T at $T=0.8$ K (Fig. 9) would fit into the calculated phase diagram only for $x_D<0.8$ K and $x_D<0.6$ K. The Dingle temperature $x_D\approx 2.6$ K of the sample not only should exclude domains at the beat *nodes*, but the domain phase *should not appear at all* in this field range, not even at the beat *maxima* when $x_D>1.78$ K.

The fact, that Eq. (5) at high fields ($H\approx 6$ T) predicts far too small values for $\chi_1(B,T)$ in beryllium, was pointed out first in Ref. 12. The present results show particularly clearly that this is true also for the low, 1–3 T field region. The amplitude of the first harmonic (and for $x_D=2.6$ K and $H=2.5$ T this is the only one to be retained, Sec. II E) is predicted to be $4\pi\chi_1\approx 2\times 0.98 R_{u=0.5,v=2.6}\approx 0.14$ for the node $\chi_1^{(l)}$ and 3 times as large for the beat antinode $\chi_1^{(h)}$. *Both of these are much below 1*. The origin of the observed large susceptibility amplitudes, much larger than predicted by the LK formula, should lie in the nearly cylindrical, quasi-two-dimensional (2D) nature of the electron ellipsoids of the Be Fermi surface. The validity of the LK formula based on the model of the 3D noninteracting electron gas is, in these conditions, to be questioned.[12]

V. CONCLUSIONS

Condon domains in beryllium were for the first time observed in a direct, spectroscopic way. The study for fields $0.9<H<3$ T *at various phases of the beat cycle* of the susceptibility amplitude $\chi_a(B)$ shows that the observed domain area in the (B,T) phase diagram is much more extended than a calculation of the susceptibility amplitude $\chi_1(B,T)$ predicts. This cannot be due to the omission of second and higher harmonics, since these should be negligibly small at the present experimental conditions ($x_D\approx 2.6$ K; $T\geqslant 0.1$ K, $B<3$ T). In particular, the observation of domains near the nodes $\chi_1=\chi_1^{(l)}$ at $H=1.992$ T and 2.739 T is difficult to explain, the calculated value of the critical parameter being $a\equiv 4\pi\chi_1=0.10\ll 1$, for example, for the first one. In other terms, to have $a>1$ at this node, the Dingle temperature of the sample should be $x_D<0.8$ K, instead of the actual value of $x_D\approx 2.6$ K. The reason why the observed χ_a is much larger than predicted is not fully understood, but the present results are consistent with that found in Ref. 12, where the enhancement of χ was attributed to the basically quasi-two-dimensionality of the electron Fermi surface.

Apart from the too small numerical values for χ_1, the theory assuming a sinusoidal $\chi(B)$ provides a qualitatively correct description of the measured $B(H)$ diagrams, Figs. 8 and 9. In particular, the data show the predicted increase of the induction difference $\Delta B(a)=8\pi M(a)$ between dia- and paramagnetic regions in the *domain phase*, and the simultaneous trend towards strong diamagnetism $-4\pi\chi(a,n)\gg 1$ in the *uniform state*, as the amplitude χ_1 moves along the beat cycle to an antinode.

The variation of the order parameter $\Delta B(T)$ (Fig. 13) is, at constant $H=B_0$ (at the center of a domain section) sharper than predicted by the theory. On reducing T from the critical T_0, the low temperature plateau of $\Delta B(T)$ appears more abruptly and lies lower than expected. No significant overheating-undercooling was observed within our accuracy of ≈ 0.2 K (Fig. 13). On the other hand, by varying H at a given temperature, the results indicate the possibility of a slight ''field-overheating'' of the order of 2 G, Fig. 10, as expected for a first order transition.

The results on the thinner sample Be-2 seem to indicate that, in spite of the estimate Eq. (19), the effective domain wall thickness w is there much larger than the cyclotron radius. This may be due to strong corrugations of the domain walls, caused by surface and bulk imperfections.

The measured μSR peak positions and relative line intensities within the doublets have provided information on the dominant, ''internal'' inductions and relative volumes of the domains. To go beyond this and determine the actual distribution of fields in the inhomogeneous wall regions would be possible only by an accurate line-shape analysis of the spectra. This is obviously limited by the experimental time and frequency resolutions: the peaks of a doublet are best separated for high (>2 T) fields ($\Delta B\lesssim\Delta H=H^2/F$) where, however, the observed amplitudes for the corresponding high precession frequencies (>270 MHz) get strongly diminished due to the finite (≈ 1 ns) time resolution. Thus, for an accurate μSR study of the interdomain regions in this case, this resolution limit should in the future be substantially lowered.

Note added. After submission of this article, a new calculation of the phase boundaries and the induction splitting ΔB, based on a 2-dimensional electron gas model, has appeared.[26] The authors confirm our conclusion that the LK formula in the present case fails to reproduce the amplitude χ_1, and show that the 2D model gives more extended domain areas, in agreement with our results.

ACKNOWLEDGMENTS

We thank Dr. E. Krasnoperov for many stimulating discussions, P.V. Likov for thermopower measurements, Dr. I.D. Reid and X. Donath for valuable help during the experiments, and the PSI staff members for providing the excellent muon beam. One of the authors (V.E.) is grateful for Grant 95-02-06015 of the Russian Fund for Fundamental Research. Thanks are due to Dr. M.A. Itskovsky for sending a copy of Ref. 26 prior to publication.

[1] J.H. Condon, Phys. Rev. **145**, 526 (1966).

[2] D. Shoenberg, *Magnetic Oscillations in Metals* (Cambridge University Press, Cambridge, England, 1984).

[3] S.C. Ying, B.J. McIntyre, and J.J. Quinn, Phys. Rev. B **2**, 1801 (1970).

[4] M.Ya. Azbel', Sov. Phys. Usp. **12**, 507 (1970).

[5] Ya. Blanter, M.I. Kaganov, and D.V. Posvyanskii, Sov. Phys. Usp. **38**, 203 (1992).

[6] R.S. Markiewicz, Phys. Rev. B **34**, 4172 (1980).
[7] A. Gordon, M.A. Itskovsky, and P. Wyder, Phys. Rev. B **55**, 812 (1997).
[8] A. Gordon, I.D. Vagner, and P. Wyder, Phys. Rev. B **41**, 658 (1990).
[9] J.H. Condon and R.E. Walstedt, Phys. Rev. Lett. **21**, 612 (1968).
[10] J.L. Smith, Ph.D. thesis, Brown University, Providence, RI, 1974.
[11] L.R. Testardi and J.H. Condon, Phys. Rev. B **1**, 3928 (1970).
[12] V.S. Egorov, Sov. Phys. Solid State **30**, 730 (1988).
[13] W.A. Reed and J.H. Condon, Phys. Rev. B **1**, 3504 (1970).
[14] V.S. Egorov, Sov. Phys. JETP **45**, 1161 (1977).
[15] G. Solt, C. Baines, V.S. Egorov, D. Herlach, E. Krasnoperov, and U. Zimmermann, Phys. Rev. Lett. **76**, 2575 (1996).
[16] G. Solt, C. Baines, V.S. Egorov, D. Herlach, E. Krasnoperov, and U. Zimmermann, Hyperfine Interact. **104**, 257 (1997).
[17] L.D. Landau and E.M Lifshitz, *Statistical Physics* (Pergamon, New York, 1980), part 2.
[18] I.A. Privorotskii, Sov. Phys. JETP **25**, 1176 (1967).
[19] I.A. Privorotskii and M.Ya. Azbel', Sov. Phys. JETP **29**, 214 (1969).
[20] M.A. Itskovsky, G.F. Kventsel, and T. Maniv, Phys. Rev. B **50**, 6779 (1994), and references therein.
[21] J.H. Tripp, P.M. Everett, W.L. Gordon, and R.W. Stark, Phys. Rev. **180**, 669 (1969).
[22] V.S. Egorov, Sov. Phys. JETP **42**, 1135 (1976).
[23] A. Schenck, *Muon Spin Rotation Spectroscopy* (Hilger, Bristol, 1986).
[24] Yu. M. Belousov and V.P. Smilga, Sov. Phys. Solid State **21**, 1416 (1979); *Proceedings of the 3rd International Symposium on Muon and Pion Interaction with Matter 1994* (JINR, Dubna, 1995).
[25] J.A. Osborn, Phys. Rev. **67**, 351 (1945).
[26] A. Gordon, M.A. Itskovsky, I.D. Vagner, and P. Wyder, Phys. Rev. Lett. **81**, 2787 (1998).